Modeling and Characterization of LiNbO3-based Microring Resonator Modulator for Synaptic Sensing

Ceren Babayigit [a], Rahim Esfandyarpour [a, b, c], Ozdal Boyraz*[a]

[a] Department of Electrical Engineering and Computer Science at the University of California, Irvine, CA 92697, USA.
[b] Department of Biomedical Engineering at the University of California, Irvine, CA 92697, USA.
[c] Department of Mechanical and Aerospace Engineering at the University of California, Irvine, CA 92697, USA.
* oboyraz@uci.edu

ABSTRACT

In neuroscience research, it is crucial to measure action potentials accurately with high spatiotemporal resolution and sensitivity. Current approaches rely on electrodes or optogenetics. New approaches providing higher spatial resolution close to a single neuron, immunity to biological noise, and lesser tissue damage during measurements are always desired. Here, we present a feasibility study on a novel label-free integrated approach by combining the electro-optic (EO) properties of lithium niobate (LN) with a microring resonator (MRR) and coherent detection to enable highly sensitive and precise measurement of action potentials. Specifically, we discuss the feasibility of this so-called opto-probe by carrying the action potential signal with light modulation and beating it through homodyne detection to detect weak signals. The MRR structure obtains the modulation of the light through the refractive index change of LN under the electric field generated by the action potential. Then, at the homodyne detection part, the action potential information is extracted from the beating of these two signals by mixing the modulated signal with a local oscillator signal. We estimate that the electric field generated by action potentials as small as 15 μV is detectable with high resolution. Furthermore, the spatial resolution of the opto-probe can reach up to 249 electrodes/mm^2 when configured as an array, which offers scalability and potential for multiplexed sensing applications. The research findings present a promising advancement towards a novel tool that overcomes the limitations of electrode-based methods, enabling highly accurate and precise measurements of action potentials and enhancing our understanding of neuronal activity in the brain.

Keywords: Lithium niobate, action potential, synaptic sensors, ring resonator modulators, electro-optic effect, optical modulators, electric field sensor.

1. INTRODUCTION

The reliable and accurate recording of electrical signals is a fundamental aspect in unraveling the intricacies of the nervous system. For the past century, neuroscience has predominantly relied on electrophysiological techniques to capture electrical signals from single neurons or populations, serving as a fundamental approach to understanding neural functioning. However, the practicality of employing electrodes is often unfeasible in many applications. In electrode-based systems, attaining high throughput proves to be a formidable challenge due to constraints in signal processing speed and data transfer rates, which can hinder the overall efficiency of these applications. Moreover, the relationship between the size of recording sites and impedance is inversely proportional, resulting in smaller electrodes being inherently noisier, displaying inferior recording quality, and possessing reduced functionality due to a decreased maximum possible stimulating current [1]. This inherent trade-off raises concerns about the long-term recording stability of such systems, adding another layer of complexity to the optimization of electrode performance in practical applications [2]. While advancements in multi-electrode array (MEA)[3,4] electronics have boosted throughput and reduced invasiveness, challenges persist due to limited electrode density and array inflexibility. Further, optogenetics, calcium imaging, and voltage-sensitive labels provide alternative ways to measure action potentials. Despite their advantages, these optical methods also face limitations, such as restricted recording duration due to photobleaching, potential generation of phototoxic free radicals, and alterations in membrane electrical properties[5]. As an additional alternative, electromagnetic field (*E*-field) sensing stands out due to its label-free

Label-free Biomedical Imaging and Sensing (LBIS) 2024, edited by Natan T. Shaked, Oliver Hayden, Proc. of SPIE Vol. 12854, 1285409 · © 2024 SPIE
1605-7422 · doi: 10.1117/12.3002839

nature, motion tolerance, immunity to interference from other radio frequency (RF) signals, and its capacity to measure a wide range of dynamic signals with a broad frequency response and high sensitivity.

In this study, we propose and examine an opto-probe design that utilizes the electro-optic (EO) effect in lithium niobate ($LiNbO_3$) to capture the electric field resulting from action potentials by sensing voltage variations in the extracellular medium. The proposed design combines the electro-optic properties of $LiNbO_3$ micro-ring resonators (MRR) with a coherent detection scheme, allowing real-time capture of synaptic activities with a μV sensitivity and spatial resolution up to 249 electrodes/mm^2. It can identify action potentials of 15μV captured by the current detector, corresponding to an electric field strength of 4.2 V/m. This presented technique enables the precise detection of subtle differences in the electric fields generated by neurons with high throughput and high-speed data transfer capabilities. It allows for recording neuronal activity without the need for external labels, all while maintaining reduced noise levels. These advancements, characterized by high efficiency and minimal interference, pave the way for exploring intricate dynamics within neuronal networks, contributing to a deeper understanding of the functioning of the nervous system.

2. THE DESIGN APPROACH AND NUMERICAL RESULTS

2.1 Structural Design

The proposed design utilizes $LiNbO_3$ MRRs to capture refractive index changes within the sensor material induced by neural activities, taking advantage of the heightened sensitivity of resonant structures to subtle disturbances. As can be seen from Figs. 1 (a) and (b), $LiNbO_3$ MRR with a double bus configuration is situated on a silicon dioxide (SiO_2) substrate, serving as a robust and stable platform with two gold electrodes designed for capturing action potentials. The first electrode, embedded in the SiO_2 layer, functions as a reference electrode. The exposed inner gold plate, serving as the second electrode, engages with the surrounding medium and neurons to capture voltages generated by neuronal activities, thus creating an electric field between the two electrodes. The internal electric field induces a refractive index change in the $LiNbO_3$ waveguide between the electrodes. This modulation of refractive index alters the input light as it traverses the MRR structure, enabling the detection of neuronal electrical activity.

Here, the outer radius of $LiNbO_3$ is adjusted as R_{out} = 20 μm, making the dimensions comparable to a single neuron's size. Light coupling in and out of the $LiNbO_3$ ring is performed by silicon nitride (Si_3N_4) bus waveguides. For single-mode operation, the widths of the $LiNbO_3$ and Si_3N_4 bus waveguides are determined using finite-difference time-domain (FDTD) mode analyses. The optimized width of the $LiNbO_3$ waveguide, yielding the highest *Q*-factor, is found to be t_2= 0.63 μm, while the widths of Si_3N_4 bus waveguides are set as t_1= 1 μm, resulting in an inner radius of R_{in} = 19.37 μm. To achieve optimal coupling between the waveguides, the gap between the $LiNbO_3$ waveguide and the Si_3N_4 bus waveguides is set to g_1= 0.15 μm. The inner gold plate, which is in contact with the exterior medium, has a radius of R_e = 17.87 μm that leaves 1.5 μm spaces (g_2) between the $LiNbO_3$ waveguide. The outer gold plate, which serves as the reference, has a thickness of t_3 = 2 μm with a spacing of g_3 = 1.5 μm from the $LiNbO_3$ waveguide. Finally, to prevent unwanted interference, the unused ends of the waveguides can be coated with perfectly matched layers (PML) or tapered.

2.2 Numerical Analyses

The sensor architecture acts as an add-drop filter, with two waveguides around a ring resonator. Optical resonance occurs at two output ports: the pass-port and the drop-port. The pass-port exhibits a transmission dip at the resonance wavelength, while the drop-port shows transmission peaks at resonant wavelengths. For focused analysis, we present results centered on the signal at the drop-port. FDTD simulations are followed by transmission measurements at the drop port. The observed spectral response of the MRR sensor reveals transmission peaks with a free spectral range (FSR) of 0.9440 THz and a *Q*-factor of 8.9756 x 10^3 (see Fig. 1(c)). Here, instead of operating at the resonance point, the proposed approach involves biasing the laser at the linear point of the transmission peak. This strategy aims to achieve a more sensitive response in detecting refractive index changes induced by the electric field. To determine this point, the derivative of the transmission peak centered at *f*=193.906 THz (point A) is calculated and illustrated in Fig. 1(d). In the figure, point B corresponding to *f*=193.951 THz, which represents the linear point that yields the highest change in the transmission output. The importance of the bias point can be rationalized by considering the resonance peak shift of the MMR sensor in response to a change in refractive index. As can be seen in Fig. 1(e), it is evident that a change in refractive index induces a blue/red shift at the output of the MRR. Leveraging this property enables the quantification of transmission changes at the drop port in relation

to variations in refractive index (see Fig. 1(f)). To check a system's response to small refractive variations due to the electric field created by action potential, one can employ a small signal analysis as shown in Fig. 1(f). Here, significant modulation changes take place when the system is biased at a point B.

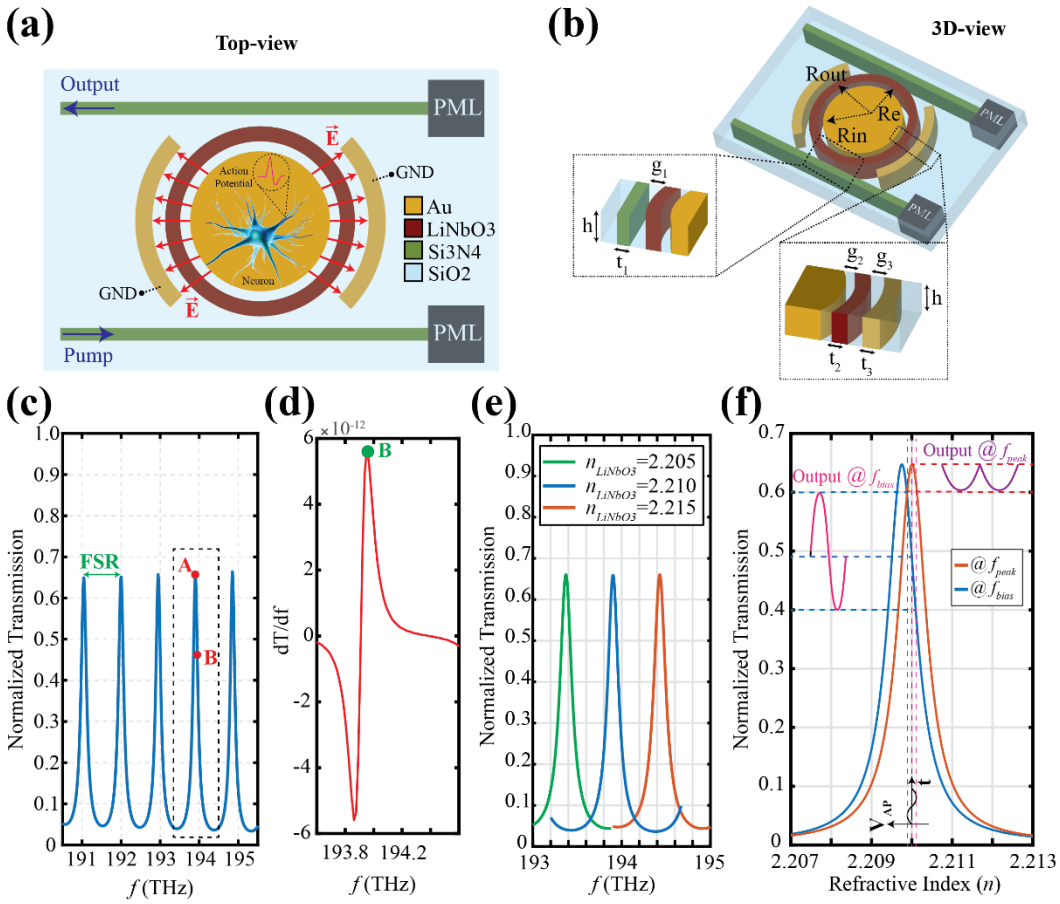

Figure 1. (a) Top view and (b) Three-dimensional schematic representation of the electro-optic ring resonator-based synaptic sensor. (c) Transmission spectra of the designed sensor. (d) Derivative of the transmission spectra with respect to frequency for a focus range. (e) Transmission spectra corresponding to different refractive indexes of an LN ring demonstrate shifts in the resonance peaks. (f) The variation in transmission concerning the refractive index of an LN ring is observed at both the resonance frequency and bias frequency.

2.3 Signal Modulation

The optical modulation of light in a microring resonator is achieved through the alteration of the resonator's refractive index. The equation describing the change in refractive index for LiNbO3 can be formulated as $n\big(V(t)\big) = (n_0 - \frac{1}{2}n_0^3 r_{13}\frac{V(t)}{d})$ where d is the spacing between the electrodes, n_o is the effective refractive index of the propagating mode, and r_{13} is the electro-optic coefficient of the $LiNbO_3$. Therefore, the neurons' action potential generates a refractive index modulation that varies over time, leading to intensity modulation in the resonator's output. At this point, the dynamic transfer function of the MMR becomes crucial in characterizing its response to time-varying input signals. If we define the static output signal as:

$$s_{out}(t) = E_{in}\frac{-(1-\tau^2)\sqrt{a}e^{j\theta(t)/2}}{\tau(1-ae^{j\theta(t)})} \quad (1)$$

Here, a is the attenuation factor, which can be expressed as a^2=exp(-αL), where α is the attenuation coefficient in the ring and L is the total circumference of the ring. The phase shift of the traveling wave is denoted by θ, *and the* self-coupling coefficient is shown as τ, where τ=τ1=τ2. Then we can define the output signal after the dynamic response as follows:

$$s_{out_{dynamic}} = A_{in}\cos(2\pi f_{in}t) + A_{in}\,\mathrm{mcos}\big(2\pi f_{m,}t + \varphi_m\big)\cos(2\pi f_{in}t). \quad (2)$$

where m(t)= $|s_{out}(t)|/A_{in}$. Therefore, the signal that varies over time at the end of the drop port, subsequent to the modulation induced by the action potential, is precisely defined by equation (2). Solving this equation allows for an accurate prediction of the LiNbO3 ring resonator's response to the action potential.

2.4 Coherent Detection

The proposed system's optical characterization involves coherent detection of the modulated signal, as depicted in the experimental scenario illustrated in Fig.2(a) with a coherent detection system. Initiating with the division of a laser beam into two branches, namely the signal beam and the reference (or local oscillator) beam, the subsequent coupling of the signal beam to the waveguide and resonator leads to the modulation induced by the neuron action potential as defined in Eq. 2. Then, both the modulated and reference beam is directed to the coherent detection system where the interfering signal beam undergoes conversion to photocurrent through a balanced detector. The resulting in differential photocurrent generated by the matched detectors is analytically expressed as follows[6]:

$$I(t) = 2R\sqrt{P_{in}P_{lo}}(\cos(\varphi_{in} + \varphi_{lo}) + m(t)\cos\big(2\pi f_{m,}t + \varphi_m + \varphi_{in} + \varphi_{lo}\big)). \quad (3)$$

By beating the modulated signal induced by the action potential with the reference signal, as represented in Eq.3, the system is capable of precise detection and quantification of neural activity. Considering neurons producing an action potential with a peak amplitude of 100 µV, as illustrated in Fig. 2 (b)-(i), the corresponding current output is calculated as in Fig. 2 (b)-(ii) by employing a narrow linewidth laser with a power value of 3mW and a relative intensity noise (RIN) value of -160 dB/Hz. This observation incorporates considerations for shot noise, thermal noise emanating from the detector, and the RIN introduced by the source laser. Here, one can see the system has the capability to detect a weak signal in the order of 100 µV with a signal-to-noise ratio (SNR) of 14.42 dB with detection bandwidths of 1kHz.

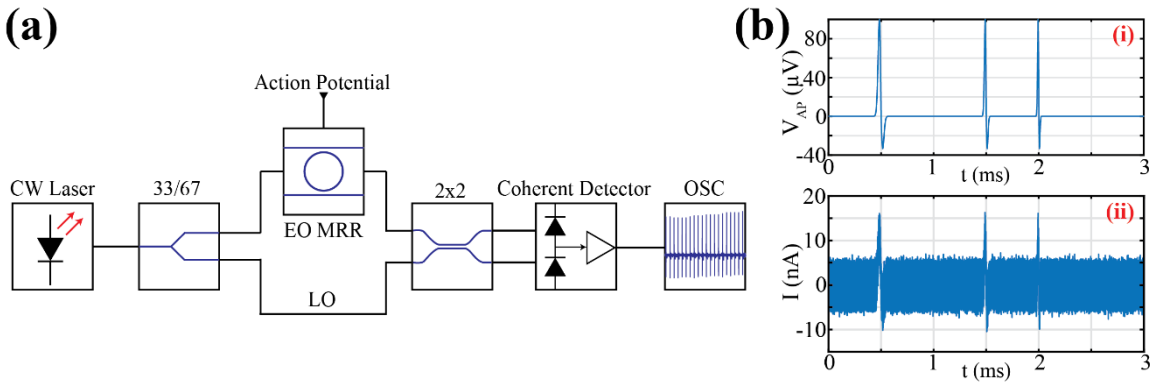

Figure 2. (a) Block diagram representing the experimental scenario for the proposed system. (b) Illustrating the system output through a case study involving (i) representative action potential data as input and (ii) the corresponding detector output.

Moreover, following the comprehensive analyses, our findings indicate that with a narrow linewidth laser having a RIN value of -160 dB/Hz, a 3dB SNR can be attained at approximately 15 µV and 147 µV action potentials by using detection bandwidths of 1 kHz and 100 kHz, respectively. Utilizing a typical telecom-grade DFB laser with a -145 dB/Hz RIN value, a 3dB SNR is achievable at around 60 µV for action potentials with a detection bandwidth of 1 kHz. In the scenario of a 100 kHz detection bandwidth, the 3 dB SNR can be reached at approximately 580 µV for action potentials. The obtained results highlight the potential efficacy of the proposed opto-probe system as a promising instrument for the precise and accurate measurement of neural activity.

3. CONCLUSION

In summary, this study introduces an opto-probe design utilizing the electro-optic effect of LiNbO3 for highly sensitive and precise action potential measurement in neuroscience research. Integrating LiNbO3's electro-optic effect with a ring resonator and coherent detection enables the detection of small refractive index changes induced by neuronal activity. The optrode surpasses current electrode-based methods with improved spatial resolution, reduced susceptibility to biological interference, and heightened sensitivity to weak signals. Analytical and numerical results demonstrate the optrode's sensitivity to microvolt-level signals. Overall, this research paves the way for developing new tools that overcome current electrode-based limitations, enabling more accurate and precise action potential measurements and enhancing our understanding of neuronal network dynamics.

REFERENCES

[1] K. M. Szostak, L. Grand, and T. G. Constandinou, "Neural Interfaces for Intracortical Recording: Requirements, Fabrication Methods, and Characteristics," *Front. Neurosci.*, vol. 11, 2017, Accessed: Jan. 05, 2024. [Online]. Available: https://www.frontiersin.org/articles/10.3389/fnins.2017.00665

[2] F. He, R. Lycke, M. Ganji, C. Xie, and L. Luan, "Ultraflexible Neural Electrodes for Long-Lasting Intracortical Recording," *iScience*, vol. 23, no. 8, p. 101387, Aug. 2020, doi: 10.1016/j.isci.2020.101387.

[3] P. K. Campbell, K. E. Jones, R. J. Huber, K. W. Horch, and R. A. Normann, "A silicon-based, three-dimensional neural interface: manufacturing processes for an intracortical electrode array," *IEEE Trans. Biomed. Eng.*, vol. 38, no. 8, pp. 758–768, Aug. 1991, doi: 10.1109/10.83588.

[4] K. D. Wise, D. J. Anderson, J. F. Hetke, D. R. Kipke, and K. Najafi, "Wireless Implantable Microsystems: High-Density Electronic Interfaces to the Nervous System," *Proc. IEEE*, vol. 92, no. 1, pp. 76–97, Jan. 2004, doi: 10.1109/JPROC.2003.820544.

[5] Y. Zhou, E. Liu, H. Müller, and B. Cui, "Optical Electrophysiology: Toward the Goal of Label-Free Voltage Imaging," *J. Am. Chem. Soc.*, vol. 143, no. 28, pp. 10482–10499, Jul. 2021, doi: 10.1021/jacs.1c02960.

[6] M. Seimetz, *High-Order Modulation for Optical Fiber Transmission*. Springer, 2009.